Constructing Simulations for DUNE

Asli Acar
Level 4 Project, MPhys
Supervisor: Professor F. Krauss
Department of Physics, Durham University
Submitted: April 25, 2022

Monte Carlo event generators have been essential in the design of high energy physics experiments and predicting new phenomena. With DUNE being realised relatively soon, simulating neutrino events has become more important than ever. We introduce our Monte Carlo event generator, developed in python by using object oriented methodologies. Our aim is to simulate particle collisions using the helicity amplitude method for matrix element calculations. We compare the helicity amplitude method to analytical methods based on completeness relations and evaluate computational efficiency and accuracy.

Contents

1. INTRODUCTION

Monte Carlo event generators are paramount to the design and analysis of high-energy scattering experiments, and are also widely exploited by theorists to make predictions for collider experiments. This makes them indispensable tools in the study of new phenomena and interpreting data from experiments in such pursuits. One of the most anticipated experiments of high energy physics that is currently under construction is DUNE, Deep Underground Neutrino Experiment. DUNE aims to investigate the origin of matter and possibly reveal relations between the stability of matter and the Grand Unification of Forces. Therefore, it is of utmost importance to simulate the interactions of neutrinos, in order to fully understand and analyse the data that will come from DUNE. Our aim is to build a Monte Carlo event generator that can tackle such tasks. We employ the helicity amplitude method in constructing matrix elements, rather than approaches based on completeness relations. This is due to the factorially increasing amount of Feynman diagrams for increasing number of final state particles making it infeasible to evaluate the amplitudes with techniques based on completeness relations. In this work, we present the helicity amplitude and spinor formalism theoretically and algorithmically, and summarise the current capabilities of our event generator. We recount all the processes that have been successfully simulated and compare the results to literature. Then, the current limitations of the algorithm are discussed and suggestions for improvements are proposed. We have used natural units throughout, and referred to incoming (outgoing) particles in collisions as $\mathrm{p}_{1,2(3,4)}$.

2. THEORETICAL BACKGROUND

A. Phase Space

The phase space is an important concept in the simulation of particle collisions. The momenta of the incoming particles are known, since these momenta are determined by the experiment set-up or chosen by the experimenter. However, for the outgoing particles, there is a variety of allowed momenta states. The phase space refers to a mathematical space that contains all of the possible momenta of all of the concerned outgoing particles. To calculate the cross section, we have to integrate over all possible final state momenta, and we do this using a phase space integral.

1. One-Particle Phase Space

Let us consider a one-particle phase space. The phase space integral has to be Lorentz invariant: inherently 4-dimensional. We also consider the fact that only positive energies are allowed for physical particles, and that the mass-shell relation has to be obeyed. So, the one-

dimensional phase space is given by [3]:

$$\mathrm{d}PS^1 = \frac{\mathrm{d}^4p}{(2\pi)^4} 2\pi\ \delta(p^2 - m^2)\theta(E) \tag{1}$$

$$= \frac{\mathrm{d}E}{(2\pi)} 2\pi\delta(E^2 - \vec{p}^2 - m^2)\theta(E)\frac{\mathrm{d}^3\vec{p}}{(2\pi)^3}$$

$$= \frac{\mathrm{d}^3\vec{p}}{2E(2\pi)^3}$$

Where 2π is a normalisation factor. The delta function implements the mass-shell relation, and positive energy solutions are ensured by using the step function.

2. Two-Particle Phase Space

It is possible to expand upon the one-dimensional phase space to create a two-dimensional phase space. We take four-momentum conservation into consideration. With proper normalisation, this can be implemented using a delta function:

$$(2\pi)^4\delta^4(p_1^\mu + p_2^\mu - (p_3^\mu + p_4^\mu)) \tag{2}$$

It is more convenient to deal with the incoming momenta in the centre of momentum frame, i.e:

$$P^\mu = p_1^\mu + p_2^\mu = (E, \vec{0}) \tag{3}$$

Where E is the total energy of the system and the three-momentum vanishes. If there is only one incoming particle, we choose the rest frame of the incoming particle. The total two-dimensional phase space is given by:

$$\mathrm{d}PS^2 = \frac{\mathrm{d}^4p_3}{(2\pi)^4} 2\pi\delta(p_3^2 - m_3^2)\theta(E_3) 2\pi\delta[(E - p_3)^2 - m_2^2]\theta(M - E_3) \tag{4}$$

$$= \frac{\mathrm{d}E_1\mathrm{d}\vec{p_3}\mathrm{d}^2\Omega_1}{(2\pi)^4}\vec{p_3}^2 2\pi\delta(E_3^2 - \vec{p_3}^2 - m_3^2)\theta(E_3) 2\pi\delta[(E - E_3)^2 - \vec{p_3}^2 - m_4^2]$$

$$= \frac{\lambda^{1/2}(M^2, m_3^2, m_4^2)}{8E^2}\frac{\mathrm{d}^2\Omega_1}{(2\pi)^2}$$

The λ function in Eq.(4) is given by:

$$\lambda(a, b, c) = (a - b - c)^2 - 4bc \tag{5}$$

If the decay products are massless, then the total phase space reduces to:

$$\int \mathrm{d}PS^2_{m=0} = \frac{1}{8\pi} \tag{6}$$

3. N-Dimensional Phase Space

The reasoning above can be applied to fit a system with N particles. For massless particles:

$$\mathrm{d}PS^n = a_n E^{2n-4} \tag{7}$$

where a_n is a dimensionless number.

B. Matrix Element Calculation

The Matrix element, also referred to as the invariant amplitude, denotes the transition probability from an initial state to a final state with definite momenta. We denote the matrix element with $\mathcal{M}$.

1. Non-Composite Particles

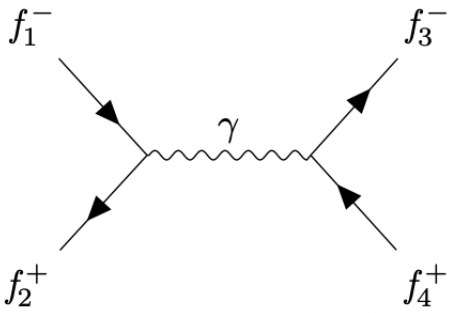

FIG. 1: Fermion scattering in the s-channel with a photon propagator.

The matrix element can be calculated by using the completeness relations and spinor matrices. Let us demonstrate by considering a process involving two incoming and two outgoing fermions,

$$f_1^-(p_1) + f_2^+(p_2) \to f_3^-(p_3) + f_4^+(p_4)$$

Where the propagator is a photon, with a coupling to the fermions:

$$ie\gamma^\mu \tag{8}$$

The Feynman diagram of the process are shown in Figure 1. We consider the s-channel, and for simplicity assume all of the particles have negligible masses. The matrix element is then given by:

$$\mathcal{M} = \bar{u}^\alpha(p_3,\lambda_3)(ie\gamma^\mu)^\beta_\alpha v(p_4,\lambda_4)_\beta \frac{-ig_{\mu\nu}}{(p_1+p_2)^2+i\epsilon}\bar{v}^\gamma(p_2,\lambda_2)(ie\gamma^\mu)^\delta_\gamma u(p_1,\lambda_1)_\delta \tag{9}$$

The spinors are represented by the usual u, $\bar{u}$, v and $\bar{v}$, and $\lambda_{1,2,3,4}$ represents the helicity of the concerned particle. Contracting the indices to simplify this expression, we find:

$$\mathcal{M} = \frac{ie^2}{s}\bar{u}(p_3,\lambda_3)\gamma^\mu v(p_4,\lambda_4)\bar{v}(p_2,\lambda_2)\gamma_\mu u(p_1,\lambda_1) \tag{10}$$
$$\mathcal{M}^\dagger = -\frac{ie^2}{s}\bar{u}(p_1,\lambda_1)\gamma_\nu v(p_2,\lambda_2)\bar{v}(p_4,\lambda_4)\gamma^\nu u(p_3,\lambda_3)$$

where $s = (p_1 + p_2)^2$. Using the completeness relations, which are given by:

$$\sum_{\lambda=\pm1} u_\alpha(p,\lambda)\bar{u}^\beta(p,\lambda) = (\not{p} + m)^\beta_\alpha \tag{11}$$
$$\sum_{\lambda=\pm1} v_\alpha(p,\lambda)\bar{v}^\beta(p,\lambda) = (\not{p} - m)^\beta_\alpha$$

We ultimately come to the conclusion:

$$\sum|\mathcal{M}|^2 = \frac{e^4}{s^2}\,\mathrm{Tr}[\not{p}_4\gamma^\nu\not{p}_3\gamma^\mu]\,\mathrm{Tr}[\not{p}_1\gamma_\nu\not{p}_2\gamma_\mu] \tag{12}$$

Evaluating the traces we find:

$$\sum\bar{\sum}|\mathcal{M}|^2 = \frac{8e^4}{s^2}[(p_1.p_4)(p_2.p_3) + (p_1.p_3)(p_2.p_4)] \tag{13}$$

Where Σ represents a sum over final state spins and $\bar{\Sigma}$ represents an average over the initial state spins.

2. *Hadrons and Form Factors*

In order to consider a scattering process that involves extended objects such as hadrons, we have to account for their inner structure by involving form factors. Lets first consider the case where unpolarised electrons scatter off a spinless charge distribution, $Ze\rho(\boldsymbol{x})$ that is normalised to unit volume [14]:

$$\int \rho(\boldsymbol{x})\,\mathrm{d}^3x = 1 \tag{14}$$

For a static target, the form factor is the Fourier transform of $\rho(\boldsymbol{x})$:

$$F(\boldsymbol{q}) = \int \rho(x)\; e^{i\boldsymbol{q}\cdot x}\,\mathrm{d}^3x \tag{15}$$

Where $\boldsymbol{q}$ is the momentum transfer between the electron and the static charge distribution. Because the matter density is normalised, $F(0) \equiv 1$. We can express the invariant amplitude as:

$$\mathcal{M} = (e\bar{u}_f\gamma_0 u_i)\frac{ZeF(\boldsymbol{q})}{|\boldsymbol{q}|^2} \tag{16}$$

However, when we have a hadron like a proton, instead of the static charge distribution model we considered, the above method cannot be applied. This is because we would then need to

consider the magnetic moment and the recoil of the proton, since the proton is not static. When we consider the elastic proton-electron collision, $e^-(p_1)\ p(p_2) \rightarrow e^-(p_3)\ p(p_4)$, we express the proton transition current as:

$$J^\mu = e\bar{u}(p_2)\left[F_1(q^2)\gamma^\mu + \frac{\mu_\mathrm{p}}{2M}F_2(q^2)i\sigma^{\mu\nu}q_\nu\right]u(p_4) \tag{17}$$

F_1 and F_2 are two form factors independent from each other, and μ_p is a constant denoting the anomalous magnetic moment of the proton. The total invariant amplitude of this scattering process is given by:

$$\mathcal{M} = \frac{e^2}{q^2}[\bar{u}(p_3)\gamma^\mu u(p_1)]\,[\bar{u}(p_2)K_\mu u(p_4)] \tag{18}$$

Where K^μ is given by:

$$K^\mu = \left[F_1(q^2)\gamma^\mu + \frac{\mu_\mathrm{p}}{2M}F_2(q^2)i\sigma^{\mu\nu}q_\nu\right] \tag{19}$$

3. Helicity Amplitude Method

The essential idea behind the helicity amplitude method is that for any given incoming and outgoing momenta and helicity combination, the scattering amplitudes are just complex numbers [5] [7]. For processes with a large number of external outgoing particles, the computational efficiency of the completeness relations based methods decrease drastically. For n number of external legs, the number of Feynman diagrams to sum over grows proportionally to $n!$, and the number of separate interferences between diagrams in the transition matrix element squared grows like $(n!)^2$. The helicity method proves to be much more efficient in this case, since we calculate any Feynman amplitude as a complex number and we can easily sum all of the Feynman amplitudes for a process at hand to square the result. In order to be able to compute this amplitude directly, one has to choose a basis. At collider energies, most masses are negligible, and massless fermions' chiralities and helicities coincide. Their chiralities are also conserved. Therefore the helicity basis is a very practical one to choose for massless fermions, as most terms vanish. To implement this method, we express the scattering amplitude in terms of scalar products of incoming and outgoing momenta and spinor products. [6] Since the momenta are known, we can easily calculate the scalar products. As we will see, the spinor products reduce to a function of momenta.

Spinors We can describe external fermions with spinors that correspond to a particular helicity λ [4] [5]:

$$\begin{aligned} \not{p}u(p,\lambda) &= \pm m u(p,\lambda) \\ \bar{u}(p,\lambda)\not{p} &= \pm m\bar{u}(p,\lambda) \end{aligned} \tag{20}$$

With p and m denoting the momentum and the mass of the particle respectively, and the negative sign refers to an anti-particle. The equations above verify the Dirac equations of motion. Additionally the spinors should fulfill:

$$(1 \mp \gamma^5 \not{s})u(p,\pm) = (1 \mp \gamma^5 \not{s})v(p,\pm) = 0 \tag{21}$$

Where s is the polarisation vector. In order to formulate spinors that obey Eq.(20-21) we introduce arbitrary spinor gauge vectors k_0 and k_1 such that:

$$\begin{aligned} k_0 \cdot k_0 &= 0, \\ k_1 \cdot k_0 &= 0, \\ k_1 \cdot k_1 &= -1 \end{aligned} \tag{22}$$

Where k_0 is time-like and k_1 is space-like. We can have independent combinations of k_0 and k_1. Thus, we can express the spinors u in terms of chiral spinors w using the spinor gauge vectors:

$$u(p,\lambda) = w(p,\lambda) + w\mu(k_0,-\lambda) \tag{23}$$

Where:

$$w(p,\lambda) = \frac{\not{p} w(k_0,-\lambda)}{\eta} \tag{24}$$

μ and η, the mass term and the normalisation, are given by:

$$\mu = \pm\frac{m}{\eta} \tag{25}$$

$$\eta = \sqrt{2(p \cdot k_0)} \tag{26}$$

Being able to choose the spinor gauge vectors is a very practical tool to have in checking the accuracy of any computation.

Essential Functions The essential functions we introduce in this section serve as building blocks in computing our amplitudes [4].

a. Chiral Projectors The chiral projectors are defined as follows:

$$\begin{aligned} P_R &= \frac{1+\gamma_5}{2} \\ P_L &= \frac{1-\gamma_5}{2} \end{aligned} \tag{27}$$

These projectors act on spinors to represent left-handed and right-handed states.

b. S-functions We define the S-function as:

$$S(\lambda, p_1, p_2) = \bar{u}(p_1,\lambda)u(p_2,-\lambda) \tag{28}$$

Using the definitions from previous sections, we can calculate S-functions:

$$S(+,p_1,p_2) = 2\frac{(p_1.k_0)(p_2.k_1) - (p_1.k_1)(p_2.k_0) + i\epsilon_{\mu\nu\rho\sigma}k_0^\mu k_1^\nu p_1^\rho p_2^\sigma}{\eta_1\eta_2} \tag{29}$$

$$S(-,p_1,p_2) = S(+,p_2,p_1)^* \tag{30}$$

c. Y, X and Z functions We construct functions to calculate spinor products [5]:

$$Y(p_1,\lambda_1;p_2,\lambda_2;c_R,c_L) = \bar{u}(p_1;\lambda_1)[c_R P_R + c_L P_L]u(p_2;\lambda_2) \tag{31}$$

$$X(p_1,\lambda_1;p_2;p_3,\lambda_3;c_R,c_L) = \bar{u}(p_1;\lambda_1)\not{p}_2[c_R P_R + c_L P_L]u(p_3;\lambda_3) \tag{32}$$

$$\begin{aligned} Z(p_1,\lambda_1;p_2,\lambda_2;p_3,\lambda_3;p_4,\lambda_4;c_R,c_L,c_R^{'},c_L^{'}) = \bar{u}(p_1,\lambda_1)\gamma^{\mu}[c_L P_L + c_R P_R]u(p_2,\lambda_2) \\ \bar{u}(p_3,\lambda_3)\gamma_{\mu}[c_L^{'} P_L + c_R^{'} P_R]u(p_4,\lambda_4) \end{aligned} \tag{33}$$

Where $c_{R,L}$ represents the right and left-handed couplings of particles with momentum $p_{1,2}$, and $c_{R,L}^{'}$ represents the right and left-handed couplings of particles with momentum $p_{3,4}$. We explicitly express these functions in terms S-functions in Tables I, II and III. Looking at a generic matrix element of the form:

$$\mathcal{M} = \frac{ie^2}{s}\bar{u}(p_1,\lambda_1)\gamma^{\mu}(c_L P_L + c_R P_R)u(p_2,\lambda_2)\bar{u}(p_3,\lambda_3)\gamma^{\mu}(c_L^{'} P_L + c_R^{'} P_R)u(p_4\lambda_4) \tag{34}$$

We observe that it can be expressed solely by a Z-function. However, for interactions that involve the exchange of a massive boson, this is not true and we need X and Y-functions.

$\boldsymbol{\lambda_1,\lambda_2}$	$\boldsymbol{Y(p_1,\lambda_1;p_2,\lambda_2;c_R,c_L)}$
$+,+$	$c_R\mu_1\eta_2 + c_L\mu_2\eta_1$
$+,-$	$c_L S(+;p_1,p_2)$

TABLE I: The explicit form of Y-functions for certain helicity combinations. The rest of the Y-functions can be acquired by exchanging $+ \leftrightarrow -$.

$\boldsymbol{\lambda_1,\lambda_2}$	$\boldsymbol{X(p_1,\lambda_1;p_2;p_3,\lambda_3;c_R,c_L)}$
$+,+$	$c_L\mu_1\eta_2^2\mu_3 + c_R(\mu_2^2\eta_1\eta_3 + S(-;p_1,p_2)S(+;p_2,p_3))$
$+,-$	$\mu_2(c_L\mu_1 S(-;p_2,p_3) + c_R\mu_3 S(-;p_1,p_2))$

TABLE II: The explicit form of X-functions for certain helicity combinations. The rest of the X-functions can be acquired by exchanging $+ \leftrightarrow -$.

$\boldsymbol{\lambda_1,\lambda_2,\lambda_3,\lambda_4}$	$\boldsymbol{Z(p_1,\lambda_1;p_2,\lambda_2;p_3,\lambda_3;p_4,\lambda_4;c_R,c_L,c_R^{'},c_L^{'})}$
$+,+,+,+$	$-2[S(+,p_3,p_1)S(-,p_4,p_2)c_R^{'}c_R - \mu_1\mu_2\eta_3\eta_4 c_R^{'}c_L - \eta_1\eta_2\mu_3\mu_4 c_L^{'}c_R]$
$+,+,+,-$	$-2\eta_2 c_R[S(+;p_4,p_1)\mu_3 c_L^{'} - S(+;p_3,p_1)\mu_4 c_R^{'}]$
$+,+,-,+$	$-2\eta_1 c_R[S(-;p_2,p_3)\mu_4 c_L^{'} - S(+;p_3,p_2)\mu_1 c_L]$
$+,+,-,-$	$-2[S(+,p_1,p_4)S(-,p_2,p_3)c_L^{'}c_R - \mu_1\mu_2\eta_3\eta_4 c_R^{'}c_L - \eta_1\eta_2\mu_3\mu_4 c_L^{'}c_R]$
$+,-,+,+$	$-2\eta_4 c_R^{'}[S(+;p_3,p_1)\mu_2 c_R - S(-;p_2,p_4)\mu_3 c_R^{'}]$
$+,-,+,-$	0
$+,-,-,+$	$-2[\mu_1\mu_4\eta_2\eta_3 c_L^{'}c_L + \mu_2\mu_3\eta_1\eta_4 c_R^{'}c_R - \mu_2\mu_4\eta_1\eta_3 c_L^{'}c_R - \mu_1\mu_3\eta_2\eta_4 c_R^{'}c_L]$
$+,-,-,-$	$-2\eta_3 c_L^{'}[S(+;p_2,p_4)\mu_1 c_L - S(+;p_1,p_4)\mu_2 c_R]$

TABLE III: The explicit form of Z-functions for certain helicity combinations. The rest of the Z-functions can be acquired by exchanging $+ \leftrightarrow -$.

C. Cross Section Calculation

The cross section is essentially a measure of probability of a process taking place, and for a process involving an n_f number of final particles and an n_i number of incoming particles it is given by:

$$\sigma_{i\to n_f} = \frac{1}{\Phi}\frac{1}{(2\pi)^{3n_f-4}}\int\left(\prod_{f=1}^{n_f}\frac{\mathrm{d}^3p_f}{2E_f}\right)\delta^4\left(\sum_{f=1}^{n_f}p_f-\sum_{i=1}^{n_i}p_i\right)|\mathcal{M}|^2 \tag{35}$$

Where Φ represents the flux, which is number of incident particles per unit area and unit time. Let us consider the scattering process with two incoming and two outgoing particles. The total cross section is obtained by integrating over all allowed momenta over the entire $(3n-4)$ dimensional phase space:

$$\sigma = \frac{1}{\Phi}\frac{1}{(2\pi)^2}\int\left(\frac{\mathrm{d}^3p_3\mathrm{d}^3p_4}{2E_3E_4}\right)\delta^4\left[(p_1+p_2)-(p_3+p_4)\right]|\mathcal{M}|^2 \tag{36}$$

In this case, the flux would be given by:

$$\Phi = 4\sqrt{(p_1.p_2)^2-m_1^2m_2^2} \tag{37}$$

The scattering probability is given by the differential cross section:

$$\left(\frac{\mathrm{d}\sigma}{\mathrm{d}\Omega}\right)_{CM} = \frac{1}{2E_1 2E_2|v_1-v_2|}\frac{|p_3|}{(2\pi)^2 4E_{CM}}|\mathcal{M}|^2 \tag{38}$$

3. THE ALGORITHM

The procedure for calculating a total cross section for a specific process is comprised of the following steps:

1. The generation of phase-space,
2. Selection and computation of the corresponding amplitude for the process,
3. The Monte Carlo integration of the phase-space and matrix element.

We will elaborate on these steps in more detail in the following subsections.

A. Phase Space Generation

Phase-space generation is the first step to simulating events. In this section, we extrapolate on how we generate the kinematics for a given process.

Isotropic Momenta Generation First of all, we select our incoming momenta. Choosing the CMS frame simplifies our task, since in this frame the total three-momentum is zero. Therefore, $\vec{p_1} = -\vec{p_2}$. Since we input E, m_1 and m_2, we can calculate the absolute value of the incoming three-momenta using the following formula:

$$|\vec{p_1}| = \lambda^{1/2}\frac{(E^2, m_1^2, m_2^2)}{2E} \tag{39}$$

Where λ is given in Eq.(5). We choose to align the momenta of particles x and y on the z-axis due to convention. So we have:

$$\vec{p_1} = (0, 0, |\vec{p_1}|) \tag{40}$$

Then, we calculate the individual energies of x and y using the mass-shell relation:

$$\begin{aligned} E_1 &= \sqrt{p_1^2 + m_1^2} \\ E_2 &= \sqrt{p_1^2 + m_2^2} \end{aligned} \tag{41}$$

We have successfully selected our incoming four-momenta in the centre of momentum frame:

$$\begin{aligned} p_1^\mu &= (E_1, \vec{p_1}) \\ p_2^\mu &= (E_2, \vec{p_2}) = (E_2, -\vec{p_1}) \end{aligned} \tag{42}$$

The composite four-momentum, p, of p_1 and p_2 is:

$$p^\mu = (E, \vec{0}) \tag{43}$$

We move on to generating outgoing four-momenta. We pick two random numbers between 0 and 1, $_1$ and $_2$, since we want the direction of our outgoing momenta to be randomised. Then, we choose our $\cos\theta$, $\sin\theta$ and ϕ such that:

$$\begin{aligned} \cos\theta &= 1 - 2_1 \\ \sin\theta &= \sqrt{1 - cos^2\theta} \\ \phi &= 2\pi_2 \end{aligned} \tag{44}$$

We choose our spherical polars to distribute momenta p_3 and p_4:

$$P(\theta, \phi) = (\sin\theta\cos\phi, \sin\theta\sin\phi, \cos\theta) \tag{45}$$

Again, since we are in the CMS frame, we have $\vec{p_3} = -\vec{p_4}$. We can calculate the absolute value of the three-momenta using Eq.(39) since we have the values of m_3 and m_4, and go through the motions of calculating individual energies once again.

$$\begin{aligned} p_1^\mu &= (E_3, |\vec{p_3}|P) = (E_3, \vec{p_3}) \\ p_2^\mu &= (E_4, |\vec{p_4}|P) = (E_4, -\vec{p_3}) \end{aligned} \tag{46}$$

Where $E_3 + E_4 = E$. In our code, the *Generator* class is responsible for generating the four-momenta in the desired frame, and calculating the corresponding flux. We will not explicitly state the steps for generation of momenta in the lab frame, since it only deviates from the above method in one step: performing a Lorentz boost after acquiring the CMS momenta.

B. Helicity Amplitudes and Matrix Element Calculations

Helicity Summation and Bit-space to Z-functions and Matrix Elements We have 2^N helicity amplitudes to sum over in order to be able to calculate the matrix element, where N stands for the number of external spinors. Our choice of basis to sum over these amplitudes are bit-space. This is possible, since the combinations of the helicities we have to sum over are:

$$\begin{aligned} H_0 &= [-1,-1,-1,-1] \to 0_2 \\ H_1 &= [-1,-1,-1,+1] \to 1_2 \\ H_2 &= [-1,-1,+1,-1] \to 10_2 \\ H_3 &= [-1,-1,+1,+1] \to 11_2 \\ H_4 &= [-1,+1,-1,-1] \to 100_2 \\ &\vdots \end{aligned}$$

These helicity combinations correspond to particular binary numbers in bit-space if we exchange $-1 \leftrightarrow 0$. By adding the binary number 1 to an element in this sequence, we are able to get the element that comes next. This is how we initialise helicity arrays, depending on how many external spinors we have. The Y, X and Z-functions receive the initialised helicity array, and relate every helicity combination to the corresponding terms. Refer to tables I, II and III for the explicit form of these functions for a given helicity combination. The terms are calculated, and then saved in an array. We then take these outputs, and use them to make specialised functions that calculate the scattering amplitude for a particular process.

C. Monte Carlo Integration

The way we compute the cross section of an event is via crude Monte Carlo Integration [8-11]. Suppose we have a one-dimensional function $f(x)$, in the range $[a, b]$ and we would like to calculate:

$$\int_a^b f(x)dx \tag{47}$$

The idea is to evaluate this function at different points in the interval $[a, b]$ and multiply with a factor of $(b - a)$, sum up all the evaluations we've obtained and average the sum, which gives us the estimated value of the integral, F:

$$F = (b-a)\frac{1}{N}\sum_{i=0}^{N} f(x_i) \tag{48}$$

In our case, we want to calculate:

$$\int d\sigma = \int |\mathcal{M}|^2(w)(\Phi) \tag{49}$$

Where w is the weight assigned to the momenta. For an isotropic $2 \to 2$ process:

$$\int dw = \int \frac{\mathrm{d}^3p_3\mathrm{d}^3p_4}{(2\pi)^4 2E_3 2E_4}\delta^4((p_1+p_2)-(p_3+p_4)) \tag{50}$$

We do the process of obtaining a matrix element from different randomised momenta, and calculating the cross section until our error is sufficiently minimised. This is achieved by a loop over loops technique: a for loop nested inside a while loop that exerts the exit condition. After the exit condition is satisfied, i.e. we have a sufficiently small error, we finally compute the total cross section as such:

$$\sigma = \frac{1}{N}\sum_{i=1}^{N}|\mathcal{M}|_i^2(w_i)(\Phi_i) \tag{51}$$

The details of error calculation for this process is given in the Appendix. The integration variable is important in determining the efficiency and accuracy of our generator, since integrating over irregular functions cause high-variance. High variance is correlated with the increase of the integration error. Therefore, we have made sure that we are integrating over a uniform function throughout this work.

4. RESULTS

Our Monte Carlo event generator is capable of simulating various $2 \rightarrow 2$ processes successfully. The current matrix library is capable of simulating:

1. $e^+e^- \rightarrow \mu^+\mu^-$ with γ and Z-boson exchanges
2. $e^-\mu^- \rightarrow e^-\mu^-$ with γ exchange
3. $e^-p \rightarrow e^-p$ with γ exchange
4. $\nu_\mu e^- \rightarrow \mu^-\nu_e$ with W-boson exchange
5. $\nu_e e^- \rightarrow \nu_e e^-$ with W-boson exchange
6. $\nu_e\, n \rightarrow e^-\, p$ with W-boson exchange
7. $\bar{\nu}_e\, p \rightarrow n\, e^+$ with W-boson exchange

The following subsections will further elaborate on the computations for some selected processes.

A. $e^+(p_1)e^-(p_2) \to \mu^+(p_3)\mu^-(p_4)$

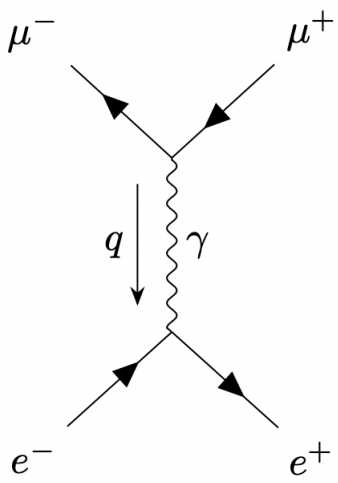

FIG. 2: Feynman diagram for electron-muon scattering.

The collision $e^+e^- \to \mu^+\mu^-$ with the mediation of a photon was the first interaction to be simulated successfully. This process is one of the simplest QED processes, since it only has one tree-level diagram and we can approximate all electron masses to zero, because $\frac{m_e}{m_\mu} \approx \frac{1}{200}$. The Feynman diagram for this process is given in Figure 2. The amplitude for our process is given by:

$$i\mathcal{M} = [\bar{v}(p_1)(-ie\gamma^\mu)u(p_2)] \left(\frac{-ig_{\mu\nu}}{q^2}\right) [\bar{u}(p_4)(-ie\gamma^\nu)v(p_3)] \tag{52}$$

$$|\mathcal{M}|^2 = \frac{e^4}{q^4}[\bar{v}(p_1)\gamma^\mu u(p_2)\bar{u}(p_2)\gamma^\nu v(p_1)][\bar{u}(p_4)\gamma_\mu v(p_3)\bar{v}(p_3)\gamma_\nu u(p_4)] \tag{53}$$

Where a bi-spinor product such as the ones we have in Eq.(52) can be complex conjugated as:

$$\begin{aligned}(\bar{v}\gamma^\mu u)^* &= u^\dagger(\gamma^\mu)^\dagger(\gamma^0)^\dagger v \\ &= u^\dagger\gamma^0\gamma^\mu v \\ &= \bar{u}\gamma^\mu v\end{aligned} \tag{54}$$

To get Eq.(53). We are still free to specify a particular spinor corresponding to any spin state desired. In most experiments the electron and positron beams are unpolarised and muon detectors are generally blind to polarisation. Therefore the measured cross section is an average over the electron-positron spins and a sum over the muon spins.

$$\sum_{\text{spins}} |M|^2 = \frac{8e^4}{q^4}\left[(p_1 \cdot p_3)(p_2 \cdot p_4) + (p_1 \cdot p_4)(p_2 \cdot p_3) + m_\mu^2(p_1 \cdot p_2)\right] \tag{55}$$

Choosing the centre of mass frame, and assuming $\sqrt{s} >> m_\mu$ we find [1]:

$$\sigma_{total} = \frac{4\pi\alpha^2}{3s} \tag{56}$$

Where α is the fine structure constant, and s is a Mandelstam variable. This is the analytic approach to calculating the cross section of the electron-muon scattering. We use the approach given in the algorithm section to generate a phase-space and calculate the Monte Carlo estimate of this cross section. The matrix element of this process can be represented by one elementary Z-function. The helicity amplitude matrix element for this collision matches up exactly to the trace calculated matrix element to the sixteenth significant figure. The ratio of the computed matrix elements using both methods was found to be 0.99.

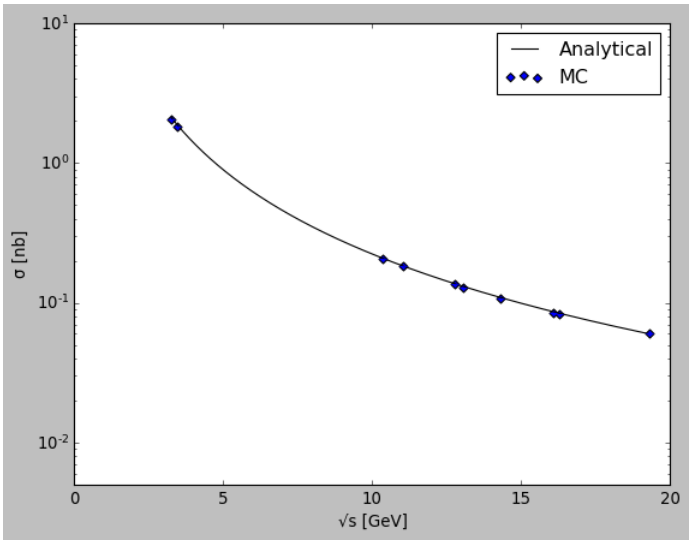

FIG. 3: Centre of mass energy dependence of the total cross section. The solid black line represents the analytic solution, $\sigma = \frac{4\pi\alpha^2}{3s}$, whereas the blue data points represent the solution computed using the Monte Carlo Method. All masses were approximated to zero.

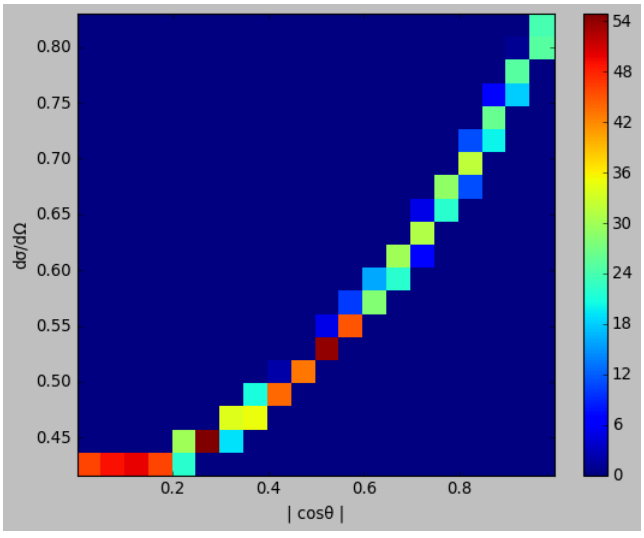

FIG. 4: Differential cross section correspondence to the scattering angle. This is a two-dimensional histogram with a colour-map that represents how many of the same $d\sigma$ value we get per bin in $|\cos\theta|$ in $N = 1000$ events. The analytic solution for the differential cross section is given in Eq.(57). We have used the definition of $d\sigma$ in Eq.(49) to obtain these results.

Figure 3 depicts the relation between the centre of mass energy and the total cross section. As one can see, the fit of the simulated model is in accordance with the analytic solution. The data trend displays a $\frac{1}{x^2}$ dependence, which is to be expected since $\sigma \propto E_{CM}^{-2}$. To obtain Figure 4, the histogram was obtained inside the while loop, where the exit condition is exerted. The analytical differential cross section of the electron muon collision is given by:

$$\frac{\mathrm{d}\sigma}{\mathrm{d}\Omega} = \frac{\alpha^2}{4E_{CM}^2}(1+\cos^2\theta) \tag{57}$$

Thus, the differential cross section is proportional to the scattering angle such that: $\frac{\mathrm{d}\sigma}{\mathrm{d}\Omega} \propto \cos^2\theta$. This is reflected in the histogram, since we observe the shape of an x^2 graph.

B. $e^-(p_1)\mu^-(p_2) \to e^-(p_3)\mu^-(p_4)$

Let us consider a closely related process to $e^+(p_1)e^-(p_2) \to \mu^+(p_3)\mu^-(p_4)$. The lowest order Feynman diagram of this process is given in Figure 5. We can take advantage of the crossing symmetry when calculating the cross section of this process.

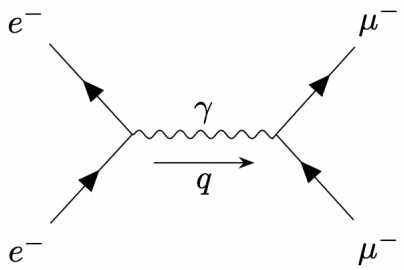

FIG. 5: Feynman diagram for $e^-\mu^- \to e^-\mu^-$

The matrix element is given by:

$$\mathcal{M} = \frac{ie^2}{q^2}[\bar{u}(p_3)\gamma^\mu u(p_1)][\bar{u}(p_4)\gamma_\mu u(p_2)] \tag{58}$$

The relation between this process and the previous one becomes clear when we consider anti-particles as particles propagating backwards in time [2]. When we exchange:

$$p_1 \leftrightarrow p_2, \quad p_3 \leftrightarrow -p_1, \quad p_2 \leftrightarrow -p_3, \quad p_4 \leftrightarrow p_4$$

We recover the $e^-(p_1)\mu^-(p_2) \to e^-(p_3)\mu^-(p_4)$ matrix element [1], which means this process is also expressed by an elementary Z-function. We calculate our analytical matrix element averaged over spins as:

$$\sum_{\text{spins}} |\mathcal{M}|^2 = \frac{2e^4(s^2+u^2)}{t^2} \tag{59}$$

Figure 6 shows the comparison between the analytical solution and the Monte Carlo cross section. The ratio of the total cross sections, analytical and Monte Carlo, was again calculated as 0.99.

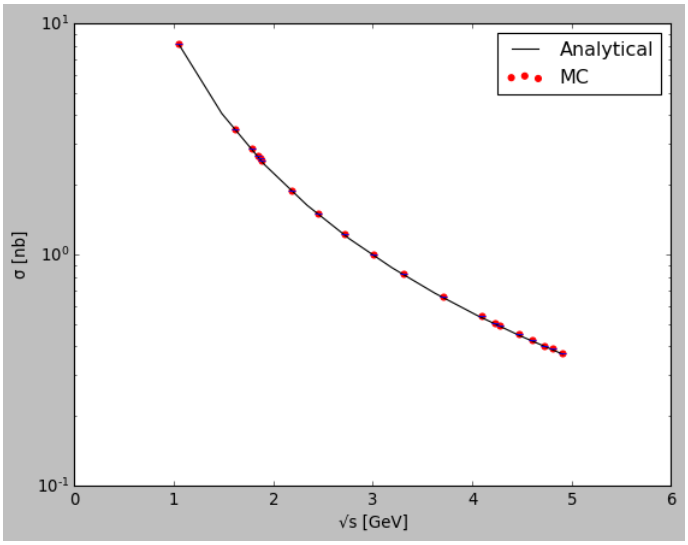

FIG. 6: Depiction of the relation between the centre of mass energy and the total cross section. The solid black line is the plot of the analytical solution and the blue data points represent the Monte Carlo simulation.

Crossing symmetry is a useful feature, since it enables us to use the same amplitude form for processes like $e^-e^+ \to \mu^+\mu^-$ and $e^-\mu^- \to e^-\mu^-$, with just a few substitutions.

C. Inverse Muon Decay: $\nu_\mu(p_1)e^-(p_2) \to \mu^-(p_3)\nu_e(p_4)$

This is the first neutrino interaction we have considered. So far, we have only considered processes propagated by photons. We now move onto consider processes propagated by massive bosons, such as the inverse muon decay. We have also successfully simulated neutrino-electron scattering, however since the simulation of that process is very similar to that of the inverse muon decay, we will not extrapolate on it. The W-boson the propagator is of the form:

$$\frac{g_{\mu\nu}}{q^2 - m_w^2} \tag{60}$$

Where m_w is the mass of the boson and q denotes the usual momentum transfer. For low energy interactions, i.e $q^2 << m_w$:

$$\frac{g_{\mu\nu}}{q^2 - m_w^2} \approx \frac{g_{\mu\nu}}{m_w^2} \tag{61}$$

The Feynman diagram for this process is given in Figure 7. The invariant amplitude is can be expressed as:

$$\mathcal{M} = \frac{g_w^2}{8}[\bar{u}(p_4)\gamma^\mu(1-\gamma_5)u(p_2)]\frac{g_{\mu\nu}}{q^2 - m_w^2}[\bar{u}(p_3)\gamma^\nu(1-\gamma_5)u(p_1)] \tag{62}$$

Where g_w is the weak coupling factor, approximated to be 0.653. We recall the definition of the projector operators, namely $P_L = \frac{1-\gamma_5}{2}$. Looking at the matrix element, and comparing it to the generic form given in Eq.(34), we see that $c_R = 0$, which is to be expected since neutrinos are left-handed: they have only one possible spin state. This also means there are only two possible spin configurations in the initial state. Left-handed interactions known as V-A theory: γ^μ gives a vector current (V), $\gamma^\mu\gamma^5$ gives an axial vector current (A). We can also write this invariant amplitude in terms of one elementary Z-function, with $c_R = c_R^{'} = 0$ and $c_L = c_L^{'} = \frac{gw}{\sqrt{2}}$. We have calculated the matrix element for this process using the helicity amplitude method and the trace method, and found their ratio to be 0.99.

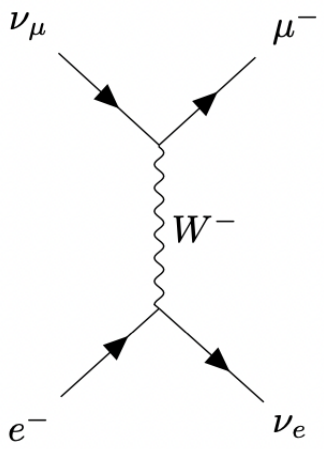

FIG. 7: Feynman diagram for inverse muon decay.

Approximating all masses to zero, the total cross section for this process is given by:

$$\sigma = \frac{1}{8}\frac{g_w^4}{m_w^4}E^2 \tag{63}$$

Where E is the CMS energy. Figure 8 plots Eq.(63) and the Monte Carlo cross section as a function of the incoming neutrino energy. As we can see the results are in agreement with the theory.

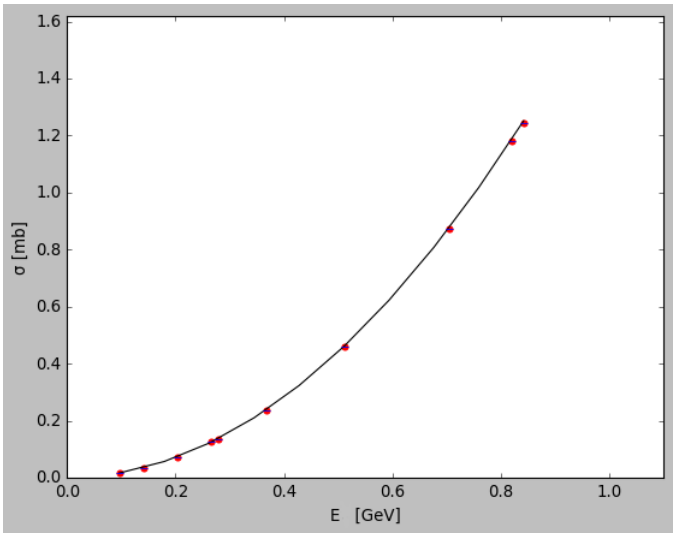

FIG. 8: Depiction of the total cross section dependence on the CMS energy, E. The solid black line plots the analytical cross section given in Eq.(63), whereas the red data points represent the Monte Carlo integration results.

D. Elastic electron-proton scattering: $e^-(p_1)p(p_2) \to e^-(p_3)p(p_4)$

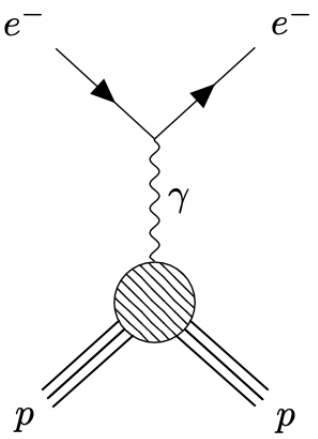

FIG. 9: The Feynman diagram for the elastic electron-proton scattering.

This is the first collision simulated that involves hadrons, thus we have to consider form factors when calculating the matrix element. We first input these form factors as just constants as a test, then assume the dipole form for proton form factors. Figure.(9) displays the Feynman diagram of the process. The invariant amplitude for this process is given in Eq.(18). We use the Gordon decomposition identity the express it as:

$$\mathcal{M} = \frac{-e^2}{q^2}[\bar{u}(p_3)\gamma^\mu u(p_1)][\bar{u}(p_4)[\gamma_\mu(F_1^{\mathrm{p}} + \mu_{\mathrm{p}}F_2^{\mathrm{p}}) - \frac{\mu_{\mathrm{p}}}{2M}(p_2 + p_4)_\mu F_2^{\mathrm{p}}]u(p_2) \tag{64}$$

Where μ_{p} is the anomalous magnetic moment of the proton. It is more practical to use linear combinations of F_1 and F_2, and so we define the Sachs form factors as:

$$G_{\mathrm{E}} = F_1^{\mathrm{p}} + \frac{\mu_{\mathrm{p}} q^2}{4M^2} F_2^{\mathrm{p}} \tag{65}$$
$$G_{\mathrm{M}} = F_1^{\mathrm{p}} + \mu_{\mathrm{p}} F_2^{\mathrm{p}}$$

These form factors are experimentally described by:

$$G_{\mathrm{E}} = \frac{1}{\left(1 - \frac{q^2}{0.71\mathrm{GeV}^2}\right)^2} \tag{66}$$
$$G_{\mathrm{M}} = \frac{\mu_{\mathrm{p}}}{\left(1 - \frac{q^2}{0.71\mathrm{GeV}^2}\right)^2}$$

The differential cross section in the lab frame for this process is given by the Rosenbluth formula:

$$\frac{\mathrm{d}\sigma}{\mathrm{d}\Omega} = \frac{\alpha^2}{4E_1^2 \sin^4\frac{\theta}{2}} \frac{E_3}{E_1} \left(\frac{G_{\mathrm{E}}^2 + \tau G_{\mathrm{M}}^2}{1+\tau} \cos^2\frac{\theta}{2} + 2\tau G_{\mathrm{M}}^2 \sin^2\frac{\theta}{2} \right) \tag{67}$$

Where:

$$\tau = -\frac{q^2}{4M} \tag{68}$$

The Monte Carlo integration in order to obtain the cross section was performed according to the method. Instead of the CMS frame, our momenta were generated in the lab frame, in order to make direct comparisons to the Rosenbluth formula. Figure 10. shows a two-dimensional histogram of the Monte Carlo integrated $\mathrm{d}\sigma$, overlapped with the Rosenbluth differential cross section against the cosine of the scattering angle. The form factors were assumed to be of the dipole form. We see that the increase in the amount of $\mathrm{d}\sigma$ with the increase in the cosine of the scattering angle is consistent with the behaviour of the line plot of the Rosenbluth differential cross section. Integrating the Rosenbluth differential cross section formula analytically, we found the ratio of the computed total cross sections to be 1.01 for an incoming massless electron energy of 1 GeV.

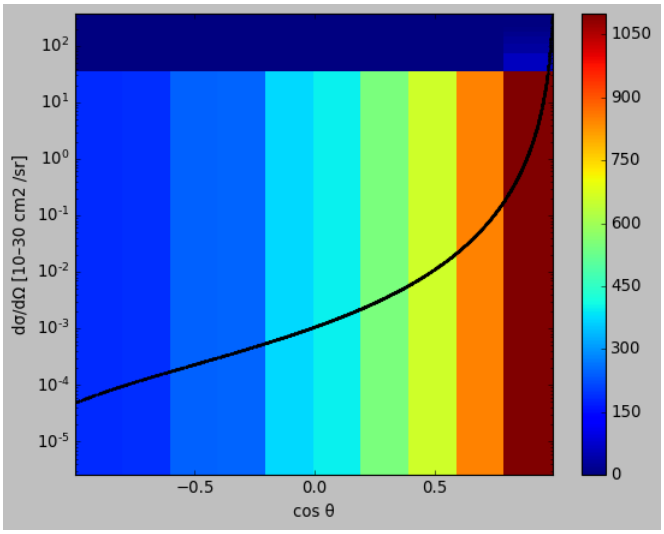

FIG. 10: The 2-dimensional histogram with bins of $\cos\theta$ corresponding to a value of the Monte Carlo estimated $\mathrm{d}\sigma$ calculated over $N = 5000$ iterations, overlapped with a line plot showing the Rosenbluth differential cross section vs $\cos\theta$. The proton mass was taken to be 0.939 GeV, whereas the electron mass was approximated to zero. The proton form factors were assumed to be of the dipole form.

E. Quasi-Elastic Neutrino Scattering: $\nu_e(p_1)\, n(p_2) \to e^-(p_3)\, p(p_4)$

This is the most complicated scattering process to be simulated so far, since it involves a more sophisticated model of form factors. We focus on charged current interactions, that are mediated by the W-boson. We use [15] , which GENIE [17] also uses for quasi-elastic neutrino interactions, to model this interaction. Namely, we define the hadronic current as:

$$\langle p(p_4)|J_\mu^+|n(p_2)\rangle = \cos\theta_c \bar{u}(p_4)\Gamma_\mu u(p_2) \tag{69}$$

Where:

$$\Gamma_\mu = \gamma_\mu F_{\mathrm{v}}^1(q^2) + \frac{i\sigma_{\mu\nu}q^\nu\zeta F_{\mathrm{v}}^2(q^2)}{2M} + \frac{q_\mu F_{\mathrm{v}}^3(q^2)}{M} + \gamma_\mu\gamma_5 F_{\mathrm{A}}(q^2) + \frac{q_\mu\gamma_5 F_{\mathrm{p}}(q^2)}{M} \tag{70}$$

$$+ \frac{\gamma_5(p_2+p_4)_\mu F_{\mathrm{A}}^3(q^2)}{M}$$

And:

$$M = \frac{m_n + m_p}{2}, \qquad \zeta = \mu_{\mathrm{p}} - \mu_{\mathrm{n}} \tag{71}$$

and q is the usual momentum transfer, and $\mu_{\mathrm{p(n)}}$ is the anomalous magnetic moment of the proton (neutron). ζ is introduced so that $F_{\mathrm{v}}^2(0) = 1$, to be consistent with the isotriplet current hypothesis. Experimental results give $\zeta = 3.71$ for beta decay with $q^2 \approx 0$. The form factors $F_{\mathrm{v}}^1, F_{\mathrm{v}}^2, F_{\mathrm{v}}^3, F_{\mathrm{A}}, F_p, F_{\mathrm{A}}^3$ respectively represent vector, weak magnetic, induced scalar, axial vector, pseudoscalar vector and induced tensor form factors. It is easy to relate this to a similar process, $\bar{\nu}_e\, p \to e^+\, n$:

$$\langle n(p_4)|J_\mu^-|p(p_2)\rangle = \cos\theta_c \bar{u}(p_4)\widetilde{\Gamma}_\mu u(p_2) \tag{72}$$

$$\widetilde{\Gamma}_{\mu}(p_2, p_4) = \gamma_0 \Gamma^{+}_{\mu}(p_4, p_2)\gamma_0 \tag{73}$$

There are some assumptions we make that lessen the amount of form factors we have to account for:

1. T-invariance asserts that all form factors have to be real.
2. The isotriplet hyphothesis implies that $F_{\rm v}^1$ and $F_{\rm v}^2$ are related to the Dirac and Pauli electromagnetic form factors respectively.
3. The principle of conserved vector current (CVC) implies that $F_{\rm v}^3 = 0$.
4. T-invariance and charge symmetry imply that $F_{\rm v}^3 = 0$ and $F_{\rm A}^3 = 0$.

Using (2) :

$$F_{\rm v}^1(q^2) = F_1^{\rm p}(q^2) - F_1^{\rm n}(q^2) \tag{74}$$

$$F_{\rm v}^2(q^2) = \frac{\mu_{\rm p} F_2^{\rm p}(q^2) - \mu_{\rm n} F_2^{\rm n}(q^2)}{\mu_{\rm p} - \mu_{\rm n}}$$

We can express $F_{\rm v}^1$ and $F_{\rm v}^2$ in terms of Sachs form factors, $G_{\rm E}$ and $G_{\rm M}$, for a more practical representation:

$$F_{\rm v}^1(q^2) = (1 - \frac{q^2}{4M^2})^{-1} \left[G_{\rm E}(q^2) - \frac{q^2}{4M^2} G_{\rm M}(q^2) \right] \tag{75}$$

$$\zeta F_{\rm v}^2(q^2) = (1 - \frac{q^2}{4M^2})^{-1} \left[G_{\rm M}(q^2) - G_{\rm E}(q^2) \right]$$

Where the Sachs form factors are given by Eq.(66). We calculate the unpolarised differential cross section of this process using the Llewellyn-Smith formula:

$$\frac{{\rm d}\sigma}{{\rm d}|q^2|} = \frac{M^2 G^2 \cos^2\theta_c}{8\pi E_\nu^2} \left[A - B\,\frac{(s-u)}{M^2} + C\,\frac{(s-u)^2}{M^4} \right] \tag{76}$$

Where s, u are Mandelstam variables. We have expressed the form factor terms with A, B and C, which are given by:

$$\begin{aligned} A = \frac{(m_e^2 - q^2)}{4M^2} \Bigg[& \left(4 - \frac{q^2}{M^2}\right) F_{\rm A}^2 - \left(4 + \frac{q^2}{M^2}\right) (F_{\rm v}^1)^2 - \frac{q^2}{M^2} (\zeta F_{\rm v}^2)^2 \left(1 + \frac{q^2}{M^2}\right) \\ & - \frac{4q^2}{M^2} F_{\rm v}^1 \zeta F_{\rm v}^2 + \frac{q^2}{M^2} \left(4 - \frac{q^2}{M^2}\right) (F_{\rm A}^3)^2 \\ & - \frac{m_e^2}{M^2} \left((F_{\rm v}^1 + \zeta F_{\rm v}^2)^2 + (F_{\rm A} + 2F_{\rm p})^2 + \left(\frac{q^2}{M^2} - 4\right) ((F_{\rm v}^3)^2 + (F_{\rm p})^2) \right) \Bigg] \end{aligned} \tag{77}$$

$$B = -\frac{q^2}{M^2}F_{\mathrm{A}}(F_{\mathrm{v}}^1 + \zeta F_{\mathrm{v}}^2) - \frac{m_e^2}{M^2}\left[\left(F_{\mathrm{v}}^1 + \frac{q^2}{4M^2}\zeta F_{\mathrm{v}}^2\right)F_{\mathrm{v}}^3 - \left(F_{\mathrm{A}} + \frac{q^2}{2M^2}F_{\mathrm{p}}\right)F_{\mathrm{A}}^3\right] \tag{78}$$

$$C = \frac{1}{4}\left(F_{\mathrm{A}}^2 + (F_{\mathrm{v}}^1)^2 - \frac{q^2}{4M^2}(\zeta F_{\mathrm{v}}^2)^2 - \frac{q^2}{M^2}(F_{\mathrm{A}}^3)^2\right) \tag{79}$$

A, B and C are of the same order of magnitude, unless they behave very differently from each other. There are some notes to be made about the form factors here:

1. The contributions from F_{p} and F_{v}^3 are of the magnitude $\approx m_e^2$. In our case, we assume that the electron mass can be approximated to zero, since it is much smaller than the proton and neutron masses. This means we fully neglect the contribution of F_{p}

2. In the approximation of setting $m_e = 0$ means the only contribution to the second class currents comes from $(F_{\mathrm{A}}^3)^2$, so distinguishing second-class currents would prove to be difficult with small form factors. This work neglects the contribution of second-class currents.

There isn't enough experimental information to determine F_{A}. We assume F_{A} is of the form:

$$F_{\mathrm{A}}(q^2) = -1.23 \cdot \left(1 - \frac{q^2}{M_A^2}\right)^{-2} \tag{80}$$

Figure 11. (12.) shows the dependence of the Monte Carlo computed cross sections for incoming (anti)neutrino to the incoming (anti)neutrino energy. The original results from [15] are given in Figure 12.

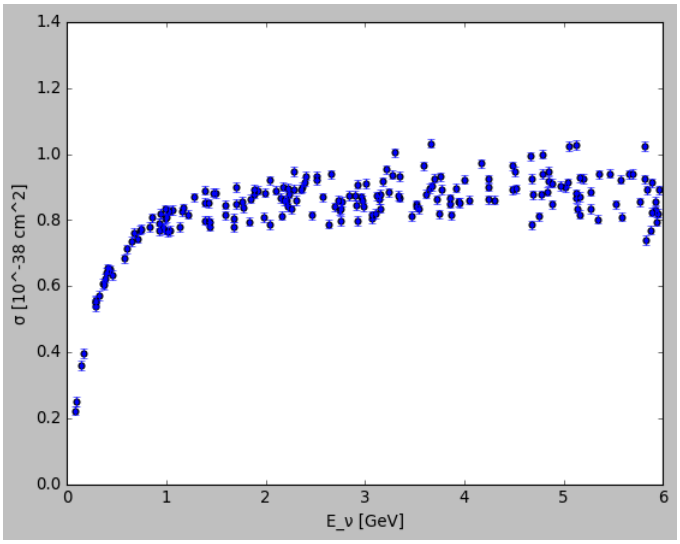

FIG. 11: The Monte Carlo integrated cross section of the process $\nu_e\ n \to e^-\ p$ for $N = 5000$ iterations with varying incoming neutrino energies in the lab frame. The proton and neutron mass were taken to be 0.939 GeV.

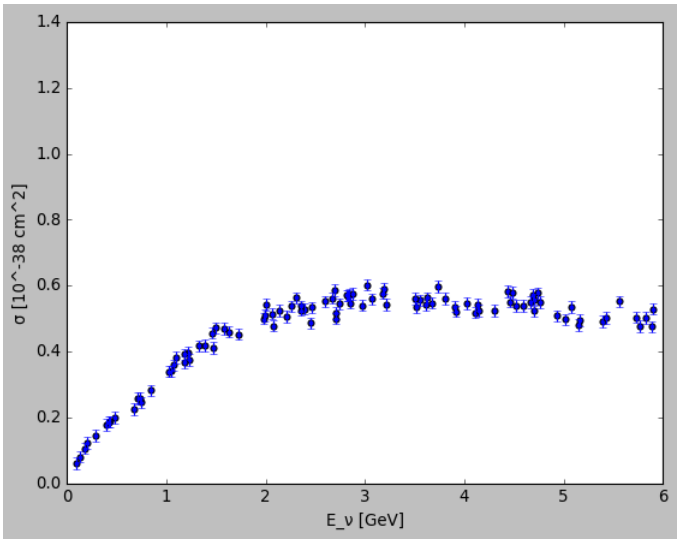

FIG. 12: The Monte Carlo integrated cross section of the process $\bar{\nu}_e\ p \rightarrow n\ e^+$ for $N = 5000$ iterations with varying incoming antineutrino energies in the lab frame. The proton and neutron mass were taken to be 0.939 GeV.

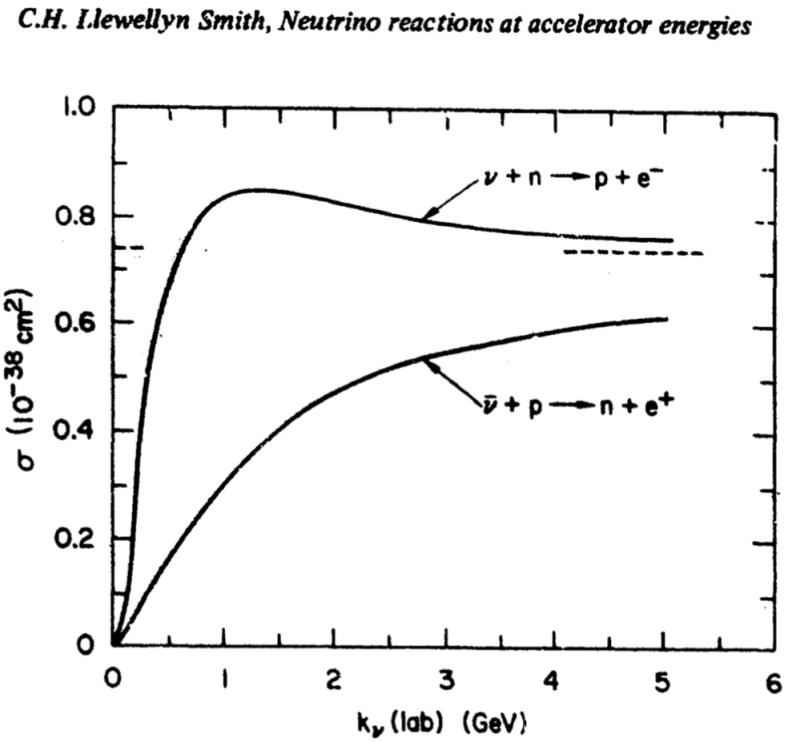

FIG. 13: Graph taken from [15] depicting the cross sections of the antineutrino and neutrino quasi-elastic scattering processes.

The Monte Carlo integrated cross sections displays the expected trends, agreeing with the Llewellyn-Smith model. The ratio of the Monte Carlo cross section to the analytical solution of the cross section at 1 GeV for $N = 1000$ iterations was computed as 1.07.

5. DISCUSSION

	Helicity Amplitude	Trace
$\bar{\nu}_e\, p \to n\, e^+$	4.35	0.147
$e^+e^- \to \mu^+\mu^-$	22.4	0.185
$\nu_\mu e^- \to \mu^-\nu_e$	44.2	0.356

TABLE IV: The computational time taken in seconds in order to calculate the total cross section at one specific CMS energy with $N = 1000$ iterations, with either the helicity amplitude method or by evaluating traces for some select processes. The efficiency comparison for the other processes scale quite similarly.

Table IV shows that we have not been able to emphasise the efficiency of the helicity amplitude method, since we have not simulated processes with a large number of final state particles. The two particle final state processes we have considered do not have a large amount of Feynman diagrams to sum over, so the trace method is more efficient than the helicity amplitude method in all of the processes that we have simulated. However, simulating these processes enable us to check the accuracy of our method, since we can easily compute the trace method solution and cross-check our results, which is useful in identifying errors in our code. So, we can move onto simulating more complex processes with the accuracy of our method confirmed.

There is much to incorporate and develop in order for our program to produce comparable results to the industry standard of Monte Carlo event generators, such as [13] and [17]. For example, we have not considered the simulation of any jets, which would require the incorporation of hadronization models into our code. So far, we have only computed unpolarised cross sections, and can only simulate interactions with 2-body final states. The next step in the development of our event generator is to consider 3-body final states, working up to the construction of an N-dimensional phase-space. When we commence working with higher dimensional phase spaces with large amount of outgoing particles, we will have to abandon our current approach of performing Monte Carlo integration over a phase space with uniform distribution. Highly dimensional phase spaces can possess structures with a lot of different strong peaks, and we would need to consider this structure in our integration. We can achieve this by adopting a multi-channel approach [5] to phase space integration, where we assign specific suitable integration channels to each Feynman diagram of the process. This method ensures the assigned channel is suited to cover the peak structure of the specific Feynman diagram in consideration, unlike the single-channel method we currently employ.

6. CONCLUSIONS

It is an exciting time for neutrino physics, and Monte Carlo event generators are more important than ever with DUNE going online in the next couple of years. In this work, we presented the current abilities of our Monte Carlo event generator. All of our results are consistent with theory, and we successfully implemented the helicity amplitude method for matrix element calculations. Our program can simulate various electromagnetic and electroweak interactions. We introduced scalar and dipole form factors, and retrieved results that are coherent with previous papers for electron-proton and quasi-elastic neutrino interactions. We compared the efficiencies of the helicity amplitude method to the trace method, however our results did not fully showcase the advantages of the helicity amplitude method, since the interactions considered in this work did not have a large number of final state particles. We acknowledged the limitations of our event generator and proposed some developmental ideas, such as adopting a multi-channel integration method.

7. ACKNOWLEDGEMENTS

The author would like to thank Professor Krauss for his support and supervision during the undertaking of the project.

References

[1] Peskin and Schroeder, *An Introduction to Quantum Field Theory*, Westview Press, (1995).

[2] Hatfield, *Quantum Field Theory of Particles and Strings*, Westview Press, (1992).

[3] Byckling and Kajantie, Particle Kinematics, Wiley-Interscience, (1973).

[4] Ballestrero, Maina and Moretti, *Heavy Quarks and Leptons at e^+e^- Colliders*, Nuclear Physics, (1994).

[5] Krauss, Kuhn and Soff, *AMEGIC++ 1.0: A Matrix Element Generator in C++*, Journal of High Energy Physics, (2002).

[6] L.J. Dixon, *A Brief Introduction to Modern Amplitude Methods*, High Energy Physics-Phenomenology, (2013).

[7] Priscila de Aquino, Will Link, Fabio Maltoni, Olivier Mattelaer, Tim Stelzer, *ALOHA: Automatic libraries of helicity amplitudes for Feynman diagram computations*, Comput. Phys. Commun., (2012).

[8] F. James, *Monte Carlo Phase Space*, (1968).

[9] Patera and Yano, *Monte Carlo Integration In a Nutshell*, MIT, (2014).

[10] Murayama, *Notes on Phase Space*, UC Berkeley, (2007).

[11] T. Evans, *Cross Sections*, Imperial, Michealmas, (2017).

[12] C.M. Becchi, G. Ridolfi, *An Introduction to Relativistic Processes and The Standard Model of Electroweak Interactions*, Springer, (2006).

[13] Enrico Bothmann et al., *Event Generation with Sherpa 2.2* , Scipost Physics, (2019).

[14] Francis Halzen, Alan D. Martin, *Quarks and Leptons: An Introductory Course in Modern Physics*, John Wiley Sons, (1984).

[15] C. H. Llewellyn-Smith, *Neutrino reactions at accelerator energies*, Physics reports, (1972).

[16] Athar, M., Singh, S., *The Physics of Neutrino Interactions*, Cambridge University Press, (2020).

[17] C. Andreopoulos and S. Gardiner, *The GENIE Neutrino Monte Carlo Generator*, (2020).

[18] Vinay Ambegaokar, *Estimating errors reliably in Monte Carlo simulations of the Ehrenfest model*, American Journal of Physics, (2010).

Appendix

A. Uniformity of Outgoing Momenta

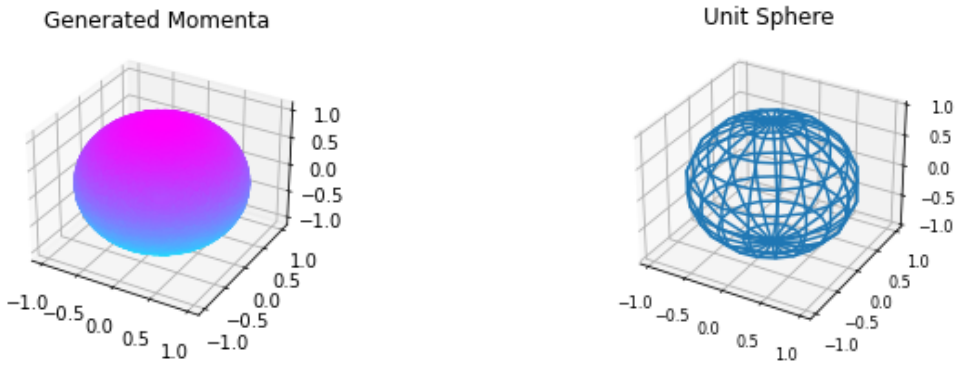

(a) **(b)**

FIG. 14

When we are generating isotropic outgoing momenta, we use random numbers that are uniformly distributed in the interval [0, 1]. To check if these momenta cover the surface of a unit sphere, we have implemented a random walk test. First of all, we generate an N number of incoming and outgoing momenta. Then, we are able to select one outgoing momenta to do the random walk test on, since we calculate our momenta in the CMS frame using massless particles, thus the other outgoing particle has the same absolute value of three-momentum and the same energy. We save the x, y and z components of the three-momentum into lists and plot a 3D graph using the module matplotlib.pyplot to get Figure 5(a). To compare this plot with the plot of a unit sphere, we plot Figure 5(b). We plot Figure 5(b) by creating functions to sample the spherical polars, and we initialise the functions with np.mgrid, with θ taking a value between [0, 2π] and ϕ taking a value between [0, π]. We calculate the volume of both Figure 5(a) and Figure 5(b) to get 1, which means our outgoing momenta cover the surface of a unit sphere.

B. Error propagation in Monte Carlo Integrations

The accuracy of the Monte Carlo integration method depends on the amount of iterations, N, we use to sample a uniformly distributed function. We denote the error, Δ, in terms of the variance, σ^2 [18]:

$$\Delta = \sqrt{\frac{\sigma^2}{N}} \tag{81}$$

Where:

$$\sigma^2 = \langle f^2 \rangle - \langle f \rangle^2 \tag{82}$$

And:

$$\langle f \rangle = \frac{1}{N} \sum_{i=1}^{N} f(x_i) \tag{83}$$

The graphs in Fig.(15) show the comparison of the analytical matrix element and the Monte Carlo matrix element calculated as a function of energy for the elastic electron-proton scattering. Figures (a) and (b) adopt scalar form factors, whereas Figures (c) and (d) adopt dipole form factors. As expected, the accuracy of the integration improves with increasing N.

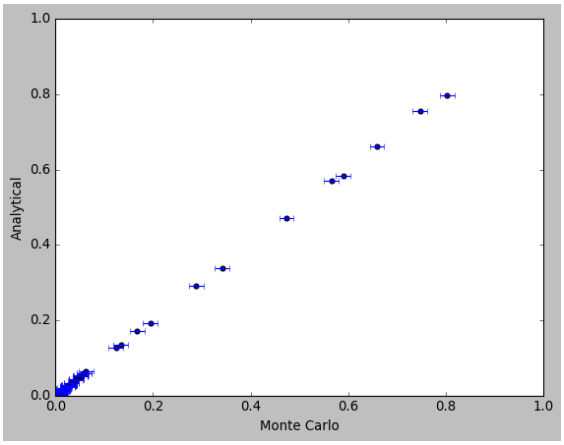

(a) The comparison of the analytical matrix element to the helicity amplitude matrix element with $F_1 = 1,\ F_2 = 1,\ N = 500$. The ratio of the matrix elements were found to be 0.987.

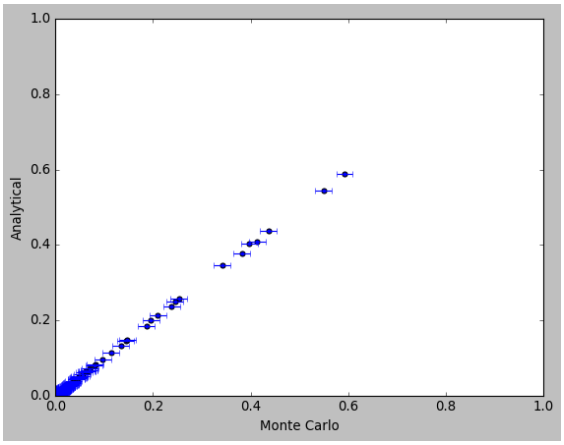

(b) The comparison of the analytical matrix element to the helicity amplitude matrix element with $F_1 = 1,\ F_2 = 1,\ N = 1000$. The ratio of the matrix elements were found to be 0.992.

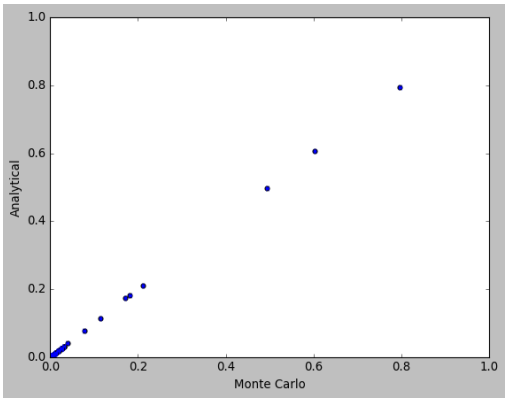

(c) The comparison of the analytical matrix element to the helicity amplitude matrix element with dipole form factors and $N = 500$.The ratio of the matrix elements were found to be 0.989.

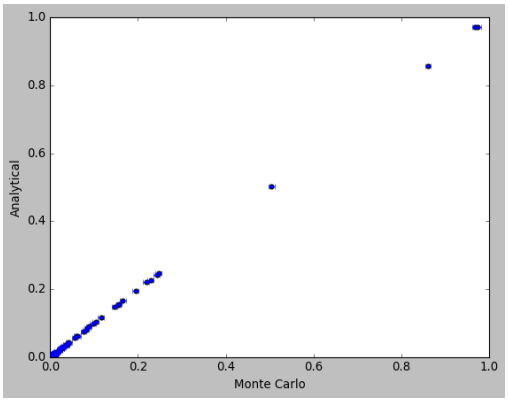

(d) The comparison of the analytical matrix element to the helicity amplitude matrix element with dipole form factors and $N = 1000$.The ratio of the matrix elements were found to be 0.993.

FIG. 15: Matrix element comparisons at $N = 500$ and $N = 1000$.